












Performance Analysis of a Distributed Optical Fiber Vibration Sensor Based on a Sagnac Interferometer

Aritz Ozcariz¹ , Guilherme Heim Weber² , Danilo Fernandes Gomes² , Igor Brutkowski Vieira da Costa² , José Rodolfo Galvão² , Victor Matheus Martins² , Daniel R. Pipa² , Marco J. Silva² ,
Jean Carlos Cardozo da Silva² , Carlos Ruiz Zamarreño¹ , Cicero Martelli² 

¹Universidad Pública de Navarra (UPNA), Arrosadía Campus, 31006 Pamplona, Navarra, Spain
aritz.ozcariz@unavarra.es, carlos.ruiz@unavarra.es

²Federal University of Technology-Paraná (UTFPR), Av. Sete de Setembro, 3165, Rebouças, CEP 80230-901, Curitiba, Paraná, Brazil

gheimweber@gmail.com, daniilofgomes@outlook.com, igor.bvc@gmail.com, jrodgalvao@gmail.com,
vm.martins09@gmail.com, danielpipa@utfpr.edu.br, mdasilva@utfpr.edu.br, jeanccs@utfpr.edu.br,
cmartelli@utfpr.edu.br

Abstract— In this work, measuring capabilities of a Sagnac Interferometer-based Distributed Optical Fiber Sensor (DOFS) system are demonstrated by comparing its results to a conventional amplitude-based Distributed Acoustic Sensing (DAS) system. Through a set of three different experiments, it was demonstrated that both sensing systems can detect and locate dynamical deformation along the fiber, in addition to determining its frequency components. The coherent amplitude-based DAS presented a lower background noise. In contrast, even though the Sagnac interferometry-based system presented low-frequency noise in the measurements, it is less susceptible to harmonic distortion for higher amplitude deformations since its sensing principles rely on the measurement of the accumulated phase rather than the amplitude of the backscattered signal purely. Accordingly, the Sagnac interferometry-based system arises as a promising and rather accessible topology for a DOFS implementation.

Index Terms— C-OTDR, Distributed Acoustic Sensing, Distributed Optical Fiber Sensing, Sagnac Interferometer.

I. INTRODUCTION

Optical fiber has proved to be a successful tool for distributed sensing applications. Several distributed optical fiber sensor (DOFS) systems have been reported in the last years [1]. The sensing principle of these systems is based on the measurement of the backscattered light (produced by Rayleigh scattering mainly) generated when optical pulses from a highly coherent light source are conducted in an optical fiber. DOFS systems are mostly based on coherent optical time domain reflectometer (C-OTDR) and phase sensitive optical time domain reflectometry (ϕ -OTDR). The difference between the two techniques is how the backscattered signal is demodulated. In the C-OTDR technique the demodulation is made by means of amplitude of the backscattered signal, whereas in the ϕ -OTDR technique the backscattered signal is demodulated by its phase. These techniques have been developed to implement vibration detection [2], distributed acoustic sensing [3], structural health monitoring [4], etc. Molenaar *et al.* [5] used the C-OTDR technique to implement a

distributed system for monitoring vibration in oil wells. The system used is called Distributed Acoustic Sensing (DAS) and uses the variations on the Rayleigh backscattering to measure the vibration. The DAS system developed had a spatial resolution of 5 m for a sensor fiber 5 km long. Another example of application using the C-OTDR technique is the detection of intruders in the security area, for example, borders [6]. The developed system had a spatial resolution of 1 km for a sensor fiber with a length of 12 km. Martins *et al.* [7] proposed a ϕ -OTDR detection scheme capable of detecting ultrasonic waves. The developed sensor was capable of measuring vibrations with a frequency of up to 39.5 kHz with a spatial resolution of 5 m on a sensor fiber with a length of 125 km. Alternatively, some DOFS systems are based on optical interferometry. Some systems have been reported based on Mach-Zehnder [8], Michelson [9] or Sagnac [10] interferometers. The study and development of such sensing systems is rather new in recent years, and it has been carried out by the search of a low cost and high-performance system for industrial applications. Pan et al [11] developed a DOFS system based on Sagnac interferometer in conjunction with an OTDR. The authors demonstrated that it is possible to detect acoustic vibrations in the optical fiber in real time. The advantage of the system is the low cost, since the light source is non-coherent. Unlike DOFS systems based on C-OTDR, the coherent trace of OTDR is produced by Sagnac's interferometer of two backscattered responses induced by the same probe pulse at two different instants of time. Therefore, the sensing system has a low requirement on the performance of the light source, significantly reducing its cost. Despite this advantage, the challenge of the system is the measurement of simultaneous multipoint vibrations in the optical fiber. Since the sensing is based on the measurement of accumulated phase of the backscattered signal of the whole optical fiber, each location response is affected by all the previous ones in terms of frequency components. In the literature, data processing techniques to solve this problem are investigated [12]–[14].

This work is motivated to support the implementation of a DOFS system using a less complex optical source and therefore more accessible technology. Sagnac-interferometry-based topology overcomes the need of a high coherence laser and opens horizons to be explored. As distributed optical sensing technology can be implemented and with less cost complexity while still maintaining reliable measurements, a large number of applications become viable. However, there are some challenges that are still unexplored in terms of measurement performance.

In this work, we demonstrate the feasibility of a system based on a Sagnac interferometer through a set of experiments to evaluate the performance of its measurements. First, the theoretical model is thoroughly studied to lay the groundwork for complete understanding. The model is validated through simulation results against real measurements. Then, we investigate the measurements performance of the Sagnac interferometer-based system compared to a conventional C-OTDR-based distributed acoustic detection (DAS) system using amplitude detection. By using such sensing system, one intends to perform the comparison of the Sagnac interferometer-based sensing system to a C-OTDR at

its simplest topology and complexity, carried by amplitude detection. The validity of the Sagnac interferometer-based DOFS as a dynamical deformation sensor and the most relevant advantages of each system are demonstrated.

II. THEORETICAL MODEL

The sensing mechanism is based on a combination of OTDR and a Sagnac interferometer-based setup. Pulsed light from a low coherence source (Fig. 1) based on superluminescent diode (SLD) is divided in two fibers with a difference in length (L_T), and then coupled back into the fiber under test (FUT). The backscattered light is propagated back through the same fibers and converted in an electrical signal in a balanced detector. The signal generated by the detector is then digitalized and processed by an algorithm in Matlab[®].

It can be deduced from a simple analysis of this setup that the backscattered light at the sensing fiber will reach the detector at three different times, depending on the path followed by both the incident light and the backscattered signal. The light following the short path for both going forth and backwards will reach the detector first and the light going both times through the long path (with the delay fiber, L_T) will reach last the detector. However, the pulse going forth through L_T and returning through the short path will reach the detector at the same time as the signal corresponding to the pulse propagating first through the short path and then backscattered through the delay fiber. Due to the low coherence of the source, these two signals, which will have propagated the same length and illuminated the same points in the FUT at different times, will be the only ones capable of generating interference.

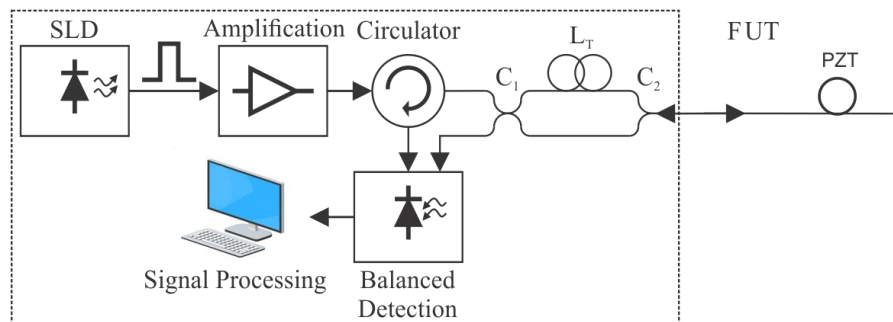


Fig. 1. Sagnac interferometer-based DOFS setup. Pulsed light from a low-coherence source is used in this interferometer-based setup in order to obtain dynamical deformation detection.

Taking into account the delay induced by L_T and the length of the FUT, L_S , the temporal window where the signal of interest will be located is between the travel time of light across the delay fiber (T_D) and T_D plus 2 times the travel time of light across the FUT (T_S) ($T_D + 2 \cdot T_S$) after each pulse is emitted, where $T_D = L_T/v_g$ and $T_S = L_S/v_g$, being v_g the speed of light in the fiber. Similarly to a conventional OTDR system, each point in time is mapped for each pulse within the specified time frame to a corresponding point along the length of the FUT. Therefore, the evolution of the backscattered signal for each pulse resembles the length domain, whereas time lapses as the pulses are launched into the FUT.

It has been demonstrated [12], [15] that the backscattered signal corresponding to the points in the fiber before any perturbation occurs is related to as

$$P_b(l) = K e^{-\alpha l} [1 + \cos(2\phi)], \quad (1)$$

where $K = (1/8) \cdot \alpha_s \cdot P_0$ is a constant related to the pulse power (P_0) and the backscattering coefficient (α_s), α is the fiber loss coefficient and ϕ is a phase difference induced by a disturbance coupled to the fiber.

If there is a perturbation at a given point in the fiber, only the signal corresponding to the segment of the fiber after such point will vary in time, according to:

$$P_b(l) = K e^{-\alpha l} \{1 + \cos[2\phi + 2\Delta\phi(l_v)]\} \quad \text{for} \quad l > l_v \quad (2)$$

where l_v is the position of the vibration in the FUT and

$$\Delta\phi(l) = \varphi(l_v/v_g) + \varphi(l_v/v_g + \Delta t_v(l)) - \varphi(l_v/v_g + \Delta t_T) - \varphi(l_v/v_g + \Delta t_T + \Delta t_v(l)) \quad (3)$$

with $\Delta t_v(l) \approx (l-l_v)/v_g$ and $\Delta t_T = L_T/v_g$ [12].

III. EXPERIMENTAL SETUP

Three experiments were designed intending to enable the comparison of performance between the Sagnac interferometry based system and the coherent based system. The first set demonstrates the capability of each system to detect and locate disturbance vibrating at constant frequency. The second test evaluates their frequency responses by performing a frequency sweep on the vibration source. The third one demonstrates the capability of each system to distinguish multiple frequency components existed within the spectrum of the evaluated signal. All the three experiments proposed use a commercial piezo-electric transducer (PZT) with 8.9 m of fiber wound as a vibration source, also known as a fiber stretcher device (model 915B Evanescent Optics Inc., shown in Fig. 3), placed approximately at 100 m of the sensing fiber (FUT) (Fig. 1 and Fig. 2). The PZT was driven by a signal generator. The Sagnac Interferometry based system and the DAS system implemented topologies are described below. In both systems the probe light pulse is launched into the sensing fiber at a repetition rate of 10 kHz. The resulting backscattered signal was digitized by a data acquisition card (DAQ) at a sampling rate of 500 MS/s within a 14-bit resolution and analyzed by an algorithm in Matlab[®]. Different pulses widths were used due to limitations on hardware of each system.

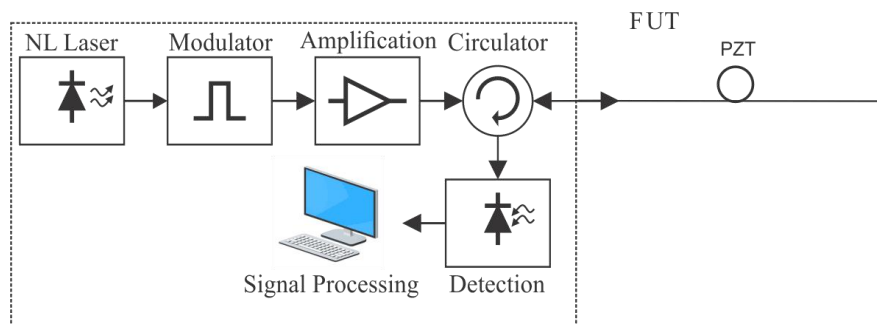


Fig. 2. Amplitude-based DAS setup. Pulsed light from a highly coherent laser source is transmitted to the FUT and the backscattered signal is detected and sampled in order to detect any vibration disturbance.

A. Sagnac Interferometry Based System

According to the setup described in Fig. 1, the pulsed light from the superluminescent light emitting diode (SLD) is amplified by an erbium doped fiber amplifier (EDFA). The light is modulated in a 500 ns wide pulse, being the narrowest width allowed within the SLD module specifications. This leads to a sensing spatial resolution of approximately 50 m. The amplified light pulse is transmitted to the wideband fiber optic coupler C_1 , where 50 % of signal is launched into path L_T with length of 1490 m and 50 % is launched into the second path with length of 2 m. The signals from the two paths are then combined by the second wideband fiber optic coupler C_2 and launched into the sensing fiber FUT with length of 460 m. The SLD has 12 mW of power, spectral width of 70 nm and center wavelength of 1550 nm. C_1 and C_2 are wideband fiber optic couplers with coupling ratio of 50:50, 2 x 2 and 2 x 1 ports, respectively. The photodetector is a balanced photodetector. Due to its high sensitivity to vibration the couplers C_1 and C_2 and the delay fiber L_T are kept in an isolated box with acoustic isolation foam.

B. Coherent Source Based System

The setup of coherent source-based system is presented in Fig. 2. The light from a high coherence laser with output power of 20 mW and spectral, central wavelength of 1550 nm and linewidth of 2 kHz (approximately 16 am) is pulsed by an Acoustic Optical Modulator (AOM), amplified by an EDFA, directed through a circulator and launched to the same sensor fiber FUT as the setup above. The pulse is 100 ns wide, providing a spatial resolution of approximately 10 m. Fig. 3 shows the fiber stretcher device used to perform the vibration excitement of a specific region of the fiber under test.

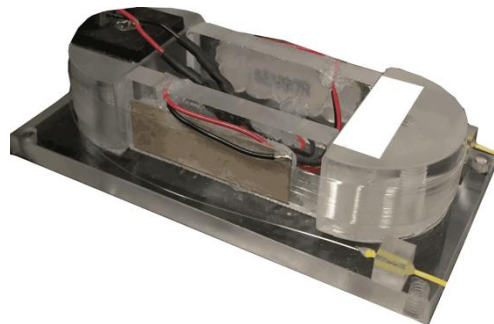


Fig. 3. Fiber stretcher device used to perform the vibration excitement of a specific region of the fiber under test.

IV. RESULTS AND DISCUSSIONS

A. Sagnac Interferometry Based System

The first test was designed to demonstrate the capability of these systems to detect and locate a vibration in the fiber and compare their performance. It consisted on applying a continuous sinusoidal signal (300 Hz) in a fiber stretcher located at a given point on the fiber and trying to reconstruct the stimulation signal from the backscattered light. This situation was simulated using the equations described in literature for the interferometer-based setup [12], [15], and adding a white noise component in order to better emulate real conditions. The corresponding experiment was performed

using the setups described above. The signals obtained with the Sagnac interferometry based system (both simulated and experimental) were processed as follows: First, for each frame consisting in the response of a single pulse, $S(l, t_i)$ the differences array was calculated by subtracting it to same signal delayed a number of samples equivalent to half the pulse width (w) as

$$D(l, t_i) = S(l, t_i) - S(l - w/2, t_i). \quad (4)$$

Due to the nature of the signal $D(l, t_i)$, a vibration point at distance l_v will be represented as a peak at $D(l_v, t_i)$. This characteristic will be used to determine the location of the vibration point along the fiber.

It should be noted that the variation in time of the signal for each point at the sampling rate of the pulse repetition can be measured.

In order to demodulate the input signal, $D(l, t)$ was first filtered and integrated in time for each point of the FUT. This procedure is expected to give as a result in $l = l_v$ a signal proportional to that of the deformation induced by the stretcher. As it can be seen on Fig. 4 (a) and Fig. 4 (b) both simulated and experimental data get a performance with good distinction of the signal in relation to the noise inherent in the measurement system. The corresponding demodulated signal is very close to the original one and its spectra clearly shows the expected frequency components.

Environmental parameters such as temperature and pressure are much more slowly than the external disturbance measured by the proposed systems, therefore, in both of them, DAS and Sagnac-based system, these parameters do not significantly affect measurements.

The same test was performed using the coherent source based OTDR and the measured data was processed according to [3], obtaining the results presented in Fig. 4 (c). It is possible to observe in this case a performance with lower noise and better spatial resolution was also obtained. The improvement in spatial resolution is due to the fact that the coherent laser is modulated with a pulse width of 100 ns, with consequent theoretical spatial resolution of approximately 10 m, a value five times smaller than the pulse width used in the optical system based on Sagnac interferometer.

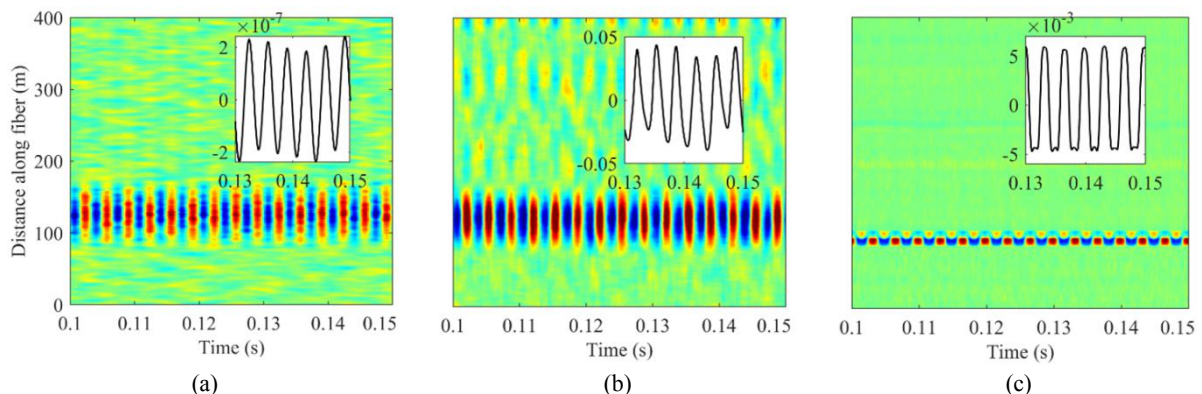


Fig. 4. Colormap representing the demodulated signals obtained for every point in the fiber and at the determined vibration point (inset) for (a) Simulated results, (b) Sagnac interferometer-based setup, and (c) Coherent DAS setup. The horizontal axis represents the temporal evolution and the vertical axis shows the position along the fiber. The vertical axis in the insets shows the amplitude of the signal in arbitrary units.

B. Frequency Sweep Analysis

It is interesting to determine the capabilities of these systems to operate under mechanical deformations at different frequencies. A test similar to the previous one was carried out, in which the fiber stretcher was submitted to a sinusoidal frequency sweep from 100 Hz to 2000 Hz in a period of 2 seconds. This allows the study of the frequency response of the system in an easy way. Fiber stretcher was driven at the same voltage level for both topologies. The signal was demodulated following the same procedure described previously. Then the spectra of the signal for subsequent time slots was calculated using an FFT algorithm, in order to observe the evolution of the frequency along time. In both cases (Fig. 5) it is possible to see good results and one can appreciate the expected behavior for 3 complete frequency sweep cycles. The evolution of the dominating peak of the FFT in time show a clear linear frequency variation between 100 and 2000 Hz, proving that both systems are capable, not only to locate a mechanical deformation of different frequencies but also to demodulate and obtain fundamental information such as frequency components of such perturbation. Some differences, however, can be seen between both tests. The Sagnac-interferometer based system setup presents a noisier signal with some low frequency noise (Fig. 5 (a)). The coherent DAS setup, on the other hand, does not show that noise band but, in contrast, some harmonic components can be seen that are not present in the Sagnac-interferometer setup (lines deriving from the starting sweep frequency in Fig. 5 (b)). The coherent DAS topology herein implemented is based on amplitude detection. It is well known that Rayleigh backscatter intensity response does not vary linearly with vibration disturbances and may imply harmonic distortion over the principal frequency component [16]–[20].

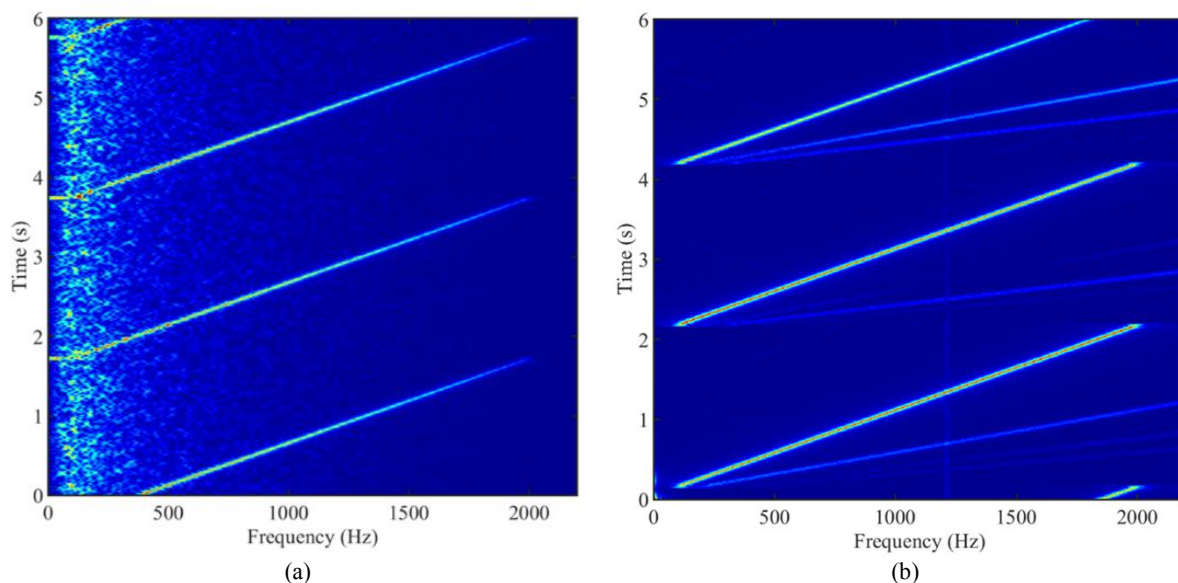


Fig. 5. Colormaps representing the evolution of the frequency components of the measured signals at the determined vibration points. (a) Sagnac-interferometer based system setup and (b) Coherent DAS setup. Colormaps are scaled in arbitrary units.

C. Amplitude Modulated Signal Analysis

Another important aspect to consider is the response to a deformation composed of different frequency components at a time. It has been determined that they are capable to distinguish single frequency components in a wide frequency range but, in order to establish the possibility to use complex analysis such as pattern recognition, it is important to study the response to composed signals. In pursuance of studying this issue, an amplitude modulated signal as an input for the fiber stretcher was used. The AM DSB-FC (amplitude modulation double-sideband full carrier) signal was configured with carrier frequency of 1000 Hz, modulation frequency to 300 Hz and set modulation index in 100%. This way, we repeated the process followed in the previous tests, and analyzed the frequency components of the measured signal. This was done for both topologies with two different amplitude values of 500 mV and 1000 mV peak to peak as input for the stretcher. According to the specifications of the fiber stretcher, the extension for a full range of driver voltage of ± 5 V is about 19 μm . Since the input voltages were at least ten times less than that, and by assuming a linear response, the deformations induced during tests were less than 2 μm . Considering a proper sampling of such bandpass signal, three frequency components are expected to be sensed, one correspondent to the carrier frequency (1000 Hz), and two more due to the modulating frequency (300 Hz): 700 and 1300 Hz. However, both sensing systems herein described acquire signals without applying a proper bandpass filter regarding the amplitude modulation. Therefore, in addition to those components it is expected to sense harmonics due to the sampling performed.

The response of the detection for a signal excitation of 500 mV and 1000 mV in the stretcher are shown in Fig. 6 and Fig. 7 respectively. On the left there are represented the results for the Sagnac-based system and the graphs on the right show the results for DAS system. The colormaps stand for the signal detected in each sensing system zoomed in the region between 0 and 200 m and at a window time of 0.05 s (Fig. 6 and Fig. 7 (a) and (b)), through which the effects of the spatial resolution performed in each case can be clearly verified. Fig. 6 and Fig. 7 (c) and (d) show the time domain signals reconstructed from the fiber stretcher position. Finally, the spectrum response of the reconstructed signal for the Sagnac-based and DAS system is presented in Fig. 6 and Fig. 7 (e) and (f) respectively. In both cases it can be seen the three expected components at 700, 1000 and 1300 Hz, and a component at 300 Hz, generated by the mixing of the signal. A low-frequency noise is explicit within the Sagnac-based system results just as verified through the previous experiments. The higher amplitude on the fiber stretcher excitation represents a benefit in this case as the signal to noise ratio rises. This effect is clearly seen on Fig. 6 (e) and Fig. 7 (e).

The results using the DAS topology show an opposite tendency as it seems to obtain a better result with lower amplitude. It can be seen how with the lower amplitude on Fig. 6 (f) that it presents basically the same frequency components as the previous setup: the three original components at 700, 1000 and 1300 Hz and a harmonic at 300 Hz. However, with a higher amplitude (Fig. 7 (f)) these signal components are almost totally overcome by the harmonics at 300 and 600 Hz.

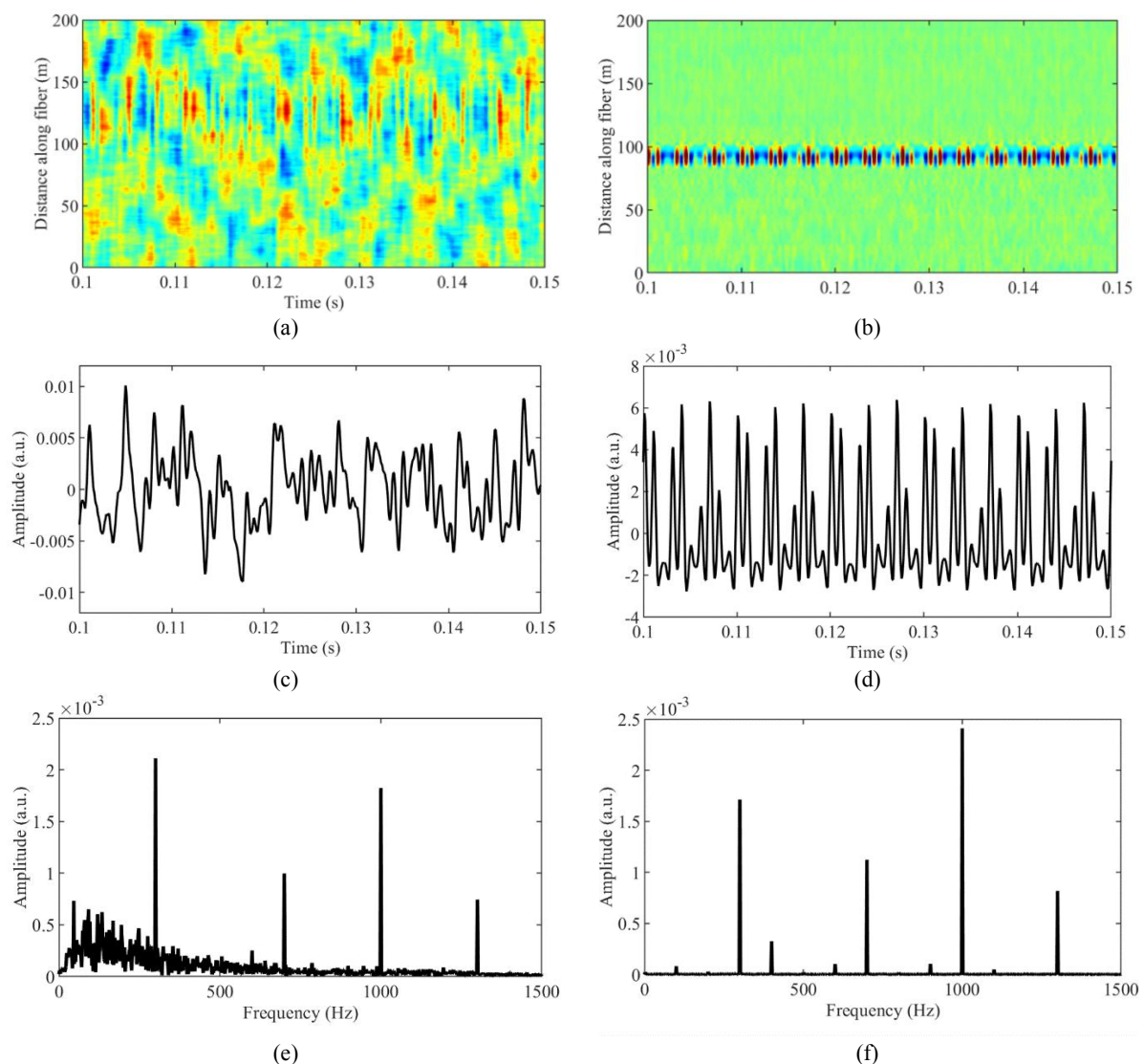


Fig. 6. Measured data using a 3-frequency component signal in the stretcher excited by a 500 mV signal using the Sagnac-interferometer based system ((a), (c) and (e)) and conventional DAS ((b), (d) and (f)). (a) and (b) show the color map representing the signal in all the FUT for a 0.05 second interval, (c) and (d) represent the temporal signal and (e) and (f) show the FFT of such signals.

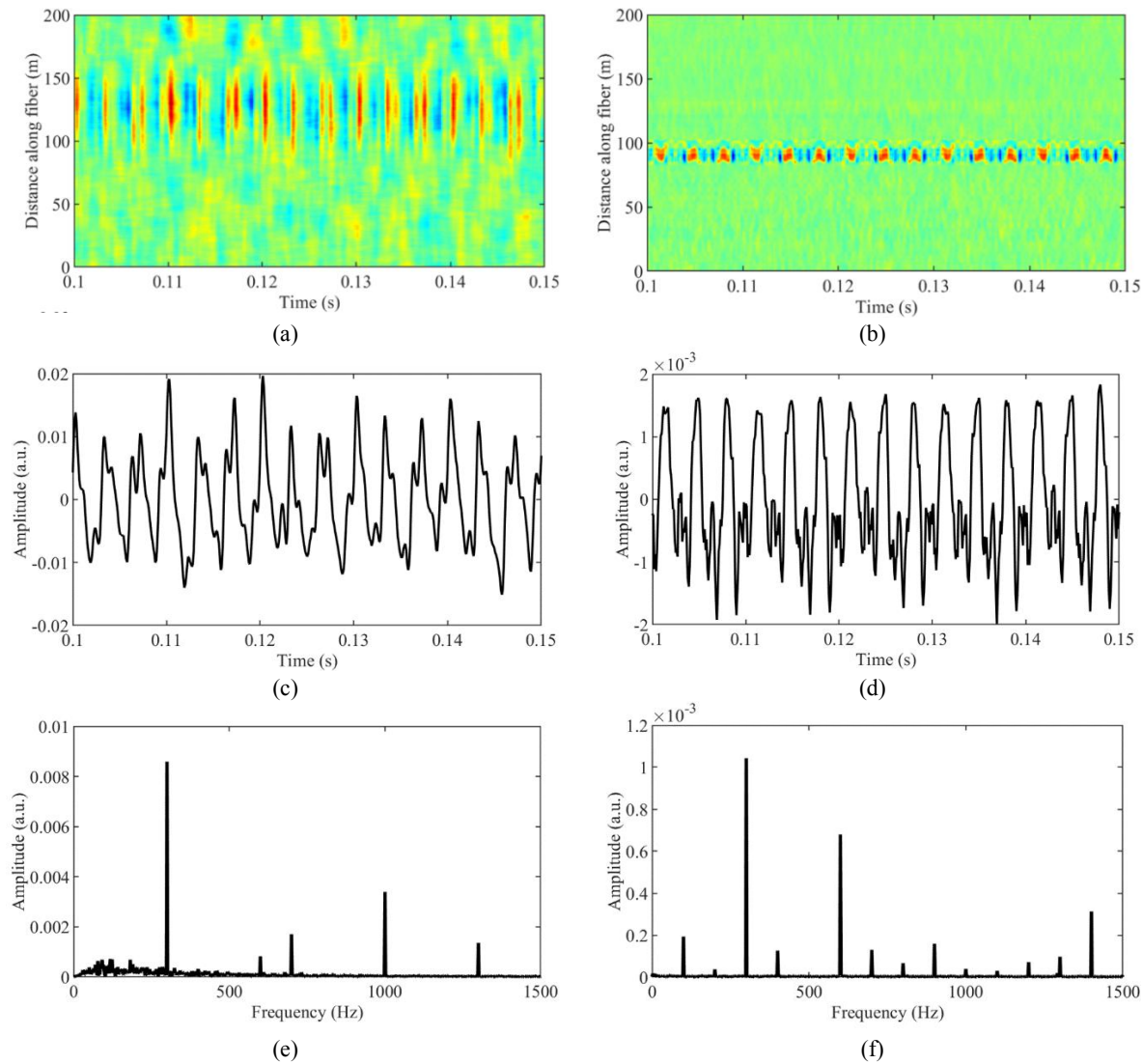


Fig. 7. Measured data using an amplitude modulated signal in the stretcher excited by a 1000 mV signal using the Sagnac-interferometer based system ((a), (c) and (e)) and conventional DAS ((b), (d) and (f)). (a) and (b) show the color map representing the signal in all the FUT for a 0.05 second interval, (c) and (d) represent the temporal signal and (e) and (f) show the FFT of such signals.

This behavior could be explained by the way signal is measured in each topology. External disturbances along the optical fiber under test induce directly changes on the phase of the backscattered signal [21]. Since coherent DAS system measures rather its amplitude, the acquired value will be a consequence of the interferometry sum of all the scatterers existed within the spatial location excited by the probe pulse. Thus, the comprehension of the resulting signal may be compromised by not knowing the limits at which the amplitude varies within the period of the backscattered wave. On the other hand, phase detection would provide a proper reconstruction of the vibration signal spectrum once the boundaries are known regarding the period and due to the use of the unwrapping algorithm [22]–[25].

The weaker the disturbance, the less will be the displacement of a given group of scatterers inside the fiber, as well as the less the amplitude will be affected by harmonic distortion. As expected, DAS

system reconstructs better a lower amplitude vibration and is more prone to saturate (and hence, create harmonic components) if the amplitude is too high. On the other side, in the interferometer based system the signal is the result of the cumulated phase along the fiber and, as a result, presents a higher noise (being worse for deformations with lower amplitude), but is not subject to as many harmonic generation for higher amplitudes as the other system.

Fig. 8 shows the simulation and results of the experiment used to evaluate system performance. In Fig. 8 (a) the fiber stretcher, located near the position of 100 m, is excited with a fixed sinusoid of 300 Hz. In the graph inset the real and simulated signal are represented for a given position in the fiber stretcher. Fig. 8 (b) shows simulated results in the frequency domain. In the graph inset, the real and simulated frequencies are presented. Red color line represents the simulated signal, and the blue color line represents the real DAS system frequency signal.

The excitation signal was also simulated for the amplitude modulation experiments, for this simulation were keeping the same characteristics of the signal applied to the fiber stretcher. The simulations results were used to calculate the performance parameters showed in Table I.

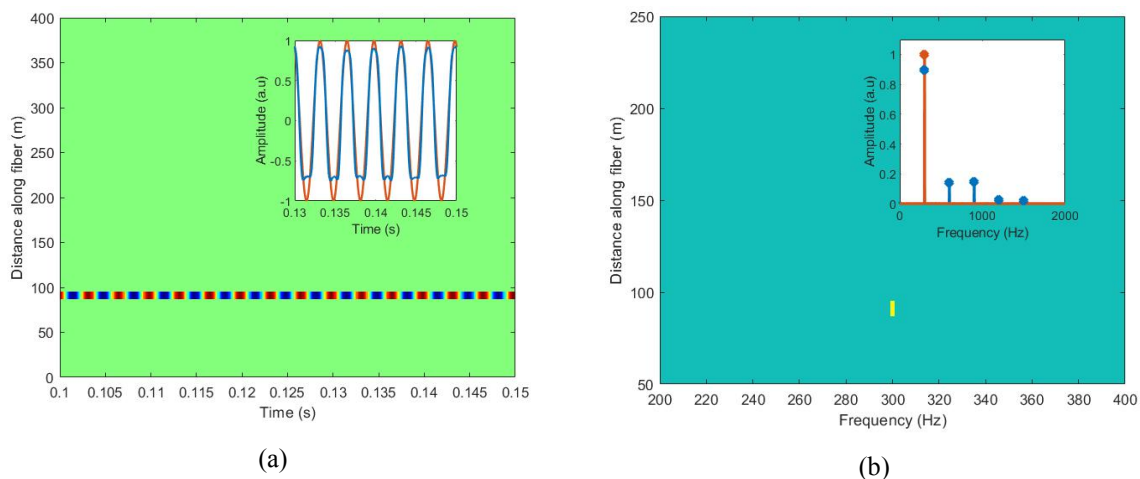


Fig. 8. Color map representing the simulated signals for each point on the fiber and at the point of vibration determined with real and simulated (inset) signal for (a) simulated signal in the time domain. The horizontal axis represents time evolution, the vertical axis represents the position along the fiber, and color scale between -1 and 1 is related to the z axis to the intensity of the resulting signals, in arbitrary units. In the inset, the horizontal axis represents the time and the vertical axis represents the amplitude for the simulated and real data. (b) simulated signal in the frequency domain. The vertical axis represents the position along the fiber and the horizontal axis is the frequency. In the inset, the horizontal axis represents the frequency and the vertical axis the amplitude for the simulated and real data.

To quantitatively evaluate the results obtained with the experiments, Table I was calculated for the experiments of single frequency at 300 Hz and amplitude modulation with modulating frequency of 300 Hz and carrier frequency at 100 Hz, this being for two different amplitudes. The results were calculated, based on a simulated waveform with the same characteristics of the signal applied to the fiber stretcher. Thus, the MSE (Mean square error) was calculated between the simulated signal and the real signal (measured with the Sagnac and the DAS distributed sensing systems).

TABLE I. QUANTITATIVE RESULTS FOR SINGLE SINUSOIDAL FREQUENCY EXPERIMENTS AT 300 HZ AND AMPLITUDE MODULATION WITH MODULATING FREQUENCY OF 300 HZ AND CARRIER AT 1000 HZ.

	All Data			Fiber Stretcher		
	MSE (Time)	MSE (Frequency)	MSE (Time)	MSE (Frequency)	SNR (dB)	THD (dBc)
Sagnac (300 Hz)	0.026	9.7E-05	0.055	4.4E-04	16.5	-18.2
DAS (300 Hz)	0.004	5.2E-06	0.026	2.2E-05	32.4	-12.8
Sagnac AM (1000 mV)	0.035	1.2E-04	0.197	6.0E-04	-	-
DAS AM (1000 mV)	0.042	2.7E-04	0.486	1.0E-03	-	-
Sagnac AM (500 mV)	0.062	6.6E-04	0.266	1.1E-03	-	-
DAS AM (500 mV)	0.005	5.6E-06	0.154	1.1E-04	-	-

The MSE values were calculated for the entire "All Data" data matrix and located only in one point of the fiber Stretcher. The MSE values, calculated in the time and in the frequency domain, are presented in Table I.

The MSE obtained for the single-frequency experiments are smaller for the DAS system than for the Sagnac-based system. In same experiments, the DAS signal to noise ratio (SNR) and harmonic distortion ratio (THD) presents higher values when compared with Sagnac-based system. As discussed in the frequency analysis results the DAS system is more susceptible to harmonic formation than Sagnac-based system.

For the amplitude modulation experiments, it's possible to verify a higher MSE value for the DAS system than for the Sagnac-based system only when the signal amplitude is higher than 1000 mV. This fact shows the appearance of harmonics and the degradation of the DAS signal for large amplitudes.

V. CONCLUSION

This work proposed a comparison of a distributed optical fiber vibration sensor based on a Sagnac interferometer with a conventional amplitude-based DAS system. Their measuring capabilities are demonstrated through a set of experiments. To promote a fair comparison both sensing systems were tested at their simplest form of implementation. It was demonstrated within three different experiments that both Sagnac-based and the conventional amplitude-based DAS are capable to detect dynamical deformation and determine the position of such event as well as its frequency components. The conventional DAS presented a lower background noise. However, the Sagnac interferometry-based system presented a better performance in recovering the frequency spectrum of the sensed signal for being less susceptible to harmonic distortion. This is due to the fact that the interferometry-based system measures accumulated phase of the backscattered signal instead of its amplitude. Even though its limitations in characterizing multiple simultaneous vibrations events in terms of frequency components, the system based on the Sagnac interferometer is suitable for applications that require the identification and location of these events.

Both sensing systems had reasonable results and allowed the characterization of the deformation

signals even to the point of recognizing different frequencies in a mixed frequencies signal, demonstrating the feasibility of the Sagnac interferometer based system on sensing distributed vibration event. In addition, the interferometer-based system enables the distributed sensing of vibrations using a less complex optical source since the interferometry topology overcomes the need of high coherence and, therefore, being a more accessible technology.

ACKNOWLEDGMENT

The authors acknowledge the financial support of the Spanish Ministry of Science and Universities (FPU15/05663), Petrobras, Brazilian National Agency of Petroleum (ANP), CAPES (Coordination of Superior Level Staff Improvement), CNPQ (National Council for Scientific and Technological Development), FINEP (Funding Authority for Studies and Projects), Araucaria Foundation, and SETI (State Secretary of Science, Technology, and Higher Education of Parana), and Multi-User Photonics Facility - UTFPR-CT.

REFERENCES

- [1] X. Bao and L. Chen, "Recent Progress in Distributed Fiber Optic Sensors," *Sensors (Switzerland)*, vol. 12, no. 7, pp. 8601–8639, 2012.
- [2] Yuelan Lu, Tao Zhu, Liang Chen, and Xiaoyi Bao, "Distributed Vibration Sensor Based on Coherent Detection of Phase-OTDR," *J. Light. Technol.*, vol. 28, no. 22, pp. 3243–3249, Nov. 2010.
- [3] C. R. Zamarreno *et al.*, "Distributed optical fiber microphone," in *Proceedings of IEEE Sensors*, 2017, vol. 2017-Decem, pp. 1–3.
- [4] S. Liehr *et al.*, "Polymer Optical Fiber Sensors for Distributed Strain Measurement and Application in Structural Health Monitoring," *IEEE Sens. J.*, vol. 9, no. 11, pp. 1330–1338, Nov. 2009.
- [5] M. M. Molenaar, D. Hill, P. Webster, E. Fidan, and B. Birch, "First Downhole Application of Distributed Acoustic Sensing for Hydraulic-Fracturing Monitoring and Diagnostics," *SPE Drill. Complet.*, vol. 27, no. 01, pp. 32–38, 2012.
- [6] K. N. Choi, J. C. Juarez, and H. F. Taylor, "Distributed fiber optic pressure/seismic sensor for low-cost monitoring of long perimeters," *Unattended Gr. Sens. Technol. Appl. V*, vol. 5090, p. 134, 2003.
- [7] H. F. Martins, S. Martin-Lopez, P. Corredera, M. L. Filograno, O. Frazao, and M. Gonzalez-Herraez, "Coherent noise reduction in high visibility phase-sensitive optical time domain reflectometer for distributed sensing of ultrasonic waves," *J. Light. Technol.*, vol. 31, no. 23, pp. 3631–3637, 2013.
- [8] S. Xie, Q. Zou, L. Wang, M. Zhang, Y. Li, and Y. Liao, "Positioning Error Prediction Theory for Dual Mach-Zehnder Interferometric Vibration Sensor," *J. Light. Technol.*, vol. 29, no. 3, pp. 362–368, Feb. 2011.
- [9] X. Hong, J. Wu, C. Zuo, F. Liu, H. Guo, and K. Xu, "Dual Michelson interferometers for distributed vibration detection," *Appl. Opt.*, vol. 50, no. 22, p. 4333, Aug. 2011.
- [10] S. J. Russell, K. R. C. Brady, and J. P. Dakin, "Real-time location of multiple time-varying strain disturbances, acting over a 40-km fiber section, using a novel dual-Sagnac interferometer," *J. Light. Technol.*, vol. 19, no. 2, pp. 205–213, 2001.
- [11] C. Pan, H. Zhu, B. Yu, Z. Zhu, and X. Sun, "Distributed optical-fiber vibration sensing system based on differential detection of differential coherent-OTDR," *Proc. IEEE Sensors*, pp. 1–3, 2012.
- [12] C. Pan, X. Liu, H. Zhu, X. Shan, and X. Sun, "Distributed optical fiber vibration sensor based on Sagnac interference in conjunction with OTDR," *Opt. Express*, vol. 25, no. 17, p. 20056, 2017.
- [13] C. Pan, H. Ye, M. Li, S. Zhao, and X. Sun, "Compensation method for blind segments of distributed optical-fiber vibration sensor based on differential-coherent otdr," *Opt. Fiber Commun. Conf. OFC 2014*, no. 1, pp. 2–4, 2014.
- [14] Y. Wang *et al.*, "Distributed acoustic sensor based on improved minimum control recursive average algorithm," *Opt. Fiber Technol.*, vol. 50, no. February, pp. 125–131, 2019.
- [15] H. Zhu, X. Shan, and X. Sun, "Analysis and demonstration of vibration waveform reconstruction in distributed optical fiber vibration sensing system," *Opt. Eng.*, vol. 56, no. 10, p. 1, 2017.
- [16] G. Tu, X. Zhang, Y. Zhang, F. Zhu, L. Xia, and B. Nakarmi, "The development of an Φ -OTDR system for quantitative vibration measurement," *IEEE Photonics Technol. Lett.*, vol. 27, no. 12, pp. 1349–1352, 2015.
- [17] G. Tu, B. Yu, S. Zhen, K. Qian, and X. Zhang, "Enhancement of Signal Identification and Extraction in a Φ -OTDR Vibration Sensor," *IEEE Photonics J.*, vol. 9, no. 1, pp. 1–10, 2017.
- [18] G. Yang, X. Fan, S. Wang, B. Wang, Q. Liu, and Z. He, "Long-Range Distributed Vibration Sensing Based on Phase Extraction from Phase-Sensitive OTDR," *IEEE Photonics J.*, vol. 8, no. 3, pp. 1–12, 2016.

- [19] L. B. Liokumovich, N. A. Ushakov, O. I. Kotov, M. A. Bisyarin, and A. H. Hartog, "Fundamentals of Optical Fiber Sensing Schemes Based on Coherent Optical Time Domain Reflectometry: Signal Model under Static Fiber Conditions," *J. Light.*
- [20] X. Fan, G. Yang, S. Wang, Q. Liu, and Z. He, "Distributed Fiber-Optic Vibration Sensing Based on Phase Extraction From Optical Reflectometry," *J. Light. Technol.*, vol. 35, no. 16, pp. 3281–3288, 2017.
- [21] S. Wang, X. Fan, Q. Liu, and Z. He, "Distributed fiber-optic vibration sensing based on phase extraction from time-gated digital OFDR," *Opt. Express*, vol. 23, no. 26, p. 33301, 2015.
- [22] K. Itoh, "Analysis of the phase unwrapping algorithm," *Appl. Opt.*, vol. 21, no. 14, p. 2470, 1982.
- [23] P. Healey, "Fading in heterodyne OTDR," *Electron. Lett.*, vol. 20, no. 1, pp. 30–32, 1984.
- [24] F. Pang *et al.*, "A Fading-Discrimination Method for Distributed Vibration Sensor Using Coherent Detection of φ -OTDR," *IEEE Photonics Technol. Lett.*, vol. 28, no. 23, pp. 2752–2755, 2016.
- [25] H. Liu *et al.*, "True Phase Measurement of Distributed Vibration Sensors Based on Heterodyne φ -OTDR," *IEEE Photonics J.*, vol. 10, no. 1, pp. 1–9, 2018